HHS Public Access

Author manuscript

Ann Biomed Eng. Author manuscript; available in PMC 2018 September 01.

Published in final edited form as:

Ann Biomed Eng. 2017 September ; 45(9): 2222–2233. doi:10.1007/s10439-017-1855-z.

An Intracardiac Soft Robotic Device for Augmentation of Blood Ejection from the Failing Right Ventricle

Markus A. Horvath[1,2,4], **Isaac Wamala**[2], **Eric Rytkin**[2], **Elizabeth Doyle**[3], **Christopher J. Payne**[1,4], **Thomas Thalhofer**[1], **Ignacio Berra**[2], **Anna Solovyeva**[2], **Mossab Saeed**[2], **Sara Hendren**[3], **Ellen T. Roche**[1,4], **Pedro J. del Nido**[2], **Conor J. Walsh**[1,4], and **Nikolay V. Vasilyev**[2]

[1]Wyss Institute for Biologically Inspired Engineering at Harvard University, Boston, MA, USA

[2]Boston Children's Hospital, Harvard Medical School, Boston, MA, USA

[3]Olin College of Engineering, Needham, MA, USA

[4]Harvard John A. Paulson School of Engineering and Applied Sciences, Cambridge, MA, USA

Abstract

We introduce an implantable intracardiac soft robotic right ventricular ejection device (RVED) for dynamic approximation of the right ventricular (RV) free wall and the interventricular septum (IVS) in synchrony with the cardiac cycle to augment blood ejection in right heart failure (RHF). The RVED is designed for safe and effective intracardiac operation and consists of an anchoring system deployed across the IVS, an RV free wall anchor, and a pneumatic artificial muscle linear actuator that spans the RV chamber between the two anchors. Using a ventricular simulator and a custom controller, we characterized ventricular volume ejection, linear approximation against different loads and the effect of varying device actuation periods on volume ejection. The RVED was then tested *in vivo* in adult pigs ($n = 5$). First, we successfully deployed the device into the beating heart under 3D echocardiography guidance ($n = 4$). Next, we performed a feasibility study to evaluate the device's ability to augment RV ejection in an experimental model of RHF ($n = 1$). RVED actuation augmented RV ejection during RHF; while further chronic animal studies will provide details about the efficacy of this support device. These results demonstrate successful design and implementation of the RVED and its deployment into the beating heart. This soft robotic ejection device has potential to serve as a rapidly deployable system for mechanical circulatory assistance in RHF.

Keywords

Right heart failure; Soft robotics; Mechanical circulatory support

Address correspondence to Nikolay V. Vasilyev, Boston Children's Hospital, Harvard Medical School, Boston, MA, USA. nikolay.vasilyev@childrens.harvard.edu.

Markus A. Horvath and Isaac Wamala have contributed equally to this work and are co-first authors.

ELECTRONIC SUPPLEMENTARY MATERIAL

The online version of this article (doi: 10.1007/s10439-017-1855-z) contains supplementary material, which is available to authorized users.

INTRODUCTION

The right ventricle (RV) of the heart pumps venous blood collected from the body to the lungs for oxygenation.[17] The RV has a crescentic shape and is bordered by a thin free wall and a rightward convex interventricular septum (IVS) (Fig. 1a). RV contraction is a complex 3-dimensional motion that includes wave-like contraction of the RV free wall, approximation of the RV free wall toward the IVS and thickening of the IVS, which results in blood ejection towards a low-resistance pulmonary vascular bed.[4,9,17]

Right heart failure (RHF) is a disease entity with diverse etiology, where RV pumping function is severely depressed.[10,11,17,27] In most cases of advanced RHF, the RV free wall and the IVS are less contractile, the RV is dilated and the septum is no longer convex shaped but rather flattened or even shifted toward the left ventricle (LV) (Fig. 1b).[6,10]

RHF is characterized by high morbidity and mortality.[15,18,27] The current treatment options include a wide spectrum of approaches, from pharmacological therapy in the early stages, to heart or heart–lung transplantation in end stage of the disease.[10,27] In advanced RHF, mechanical circulatory support (MCS) has become a valuable therapeutic solution, when a donor organ is not available. The state of the art among MCS devices is one-way flow pumps that divert blood returning from the body to pulmonary vasculature.[1,12]

We present an alternative approach where a soft robotic pneumatic artificial muscle (PAM) is deployed across the failing RV free wall and IVS to augment their approximation during systole, leading to ejection of additional blood volume from the RV (Figs. 1c and 1d). Thus, pulsatile flow augmentation is achieved across the native cardiovascular vasculature without diverting blood flow through an artificial circuit.

McKibben PAMs have been shown to have force contraction characteristics similar to muscle[7,8] and have demonstrated the ability to support the failing heart by closely mimicking the contractile motion of the heart.[22,23] In contrast to previous designs that provide compressive biventricular support on the heart surface, the proposed RVED operates inside the RV, specifically addressing the structural changes that are seen in RHF.[20] A low profile device such as this, which can be easily deployed into the beating heart under echocardiography guidance, may be very well suited for the short-term support of a failing RV. Here we present the design and fabrication of the device, as well as *ex vivo* and *in vivo* testing in a porcine animal model.

MATERIALS AND METHODS

Device Design and Fabrication

The RVED is comprised of four major components: a linear actuator, a septal anchoring system, an RV free wall anchoring system and seal (Figs. 1c, 1d, and 1e), and a controller. We approached the device design by addressing each component separately. For each component, we defined the functional requirements, and then developed engineering solutions.

Linear Actuator—The linear actuator is a modified McKibben PAM that consists of an inflatable inner bladder constrained by a braided polyethylene terephthalate (PET) mesh. When the inner bladder of the actuator is inflated its radial expansion is constrained by the outer mesh, which results in linear contraction (Fig. 1d).[20] The PAM is customized for intracardiac use by fabricating it entirely from polymer materials to allow echocardiography guided placement into the beating heart and by the addition of an outer bladder that isolates the device from the blood (Fig. 1e). Additionally, applying vacuum to the outer bladder during RV diastole, while the internal bladder is deflated, facilitates PAM extension and minimizes the device volume thus allowing RV diastolic filling. Both bladders are actuated independently through a double lumen airline (Fig. 1e) attached to a custom control system.

Previously suggested PAMs for cardiac support provided up to 24% linear contraction at a total length of 140 mm.[19] Roche *et al.* described the use of non-compliant thermoplastic polyurethane (TPU) bladders to improve reliability while providing up to 34% linear contraction in a 120 mm long PAM for cardiac assist.[21] To meet the specifications of the required intracardiac use, the PAM was customized to a 10 mm maximum width and 40 mm length which was the lower limit of a dilated human RV.[5,14] To match the typical free wall to IVS approximation distance seen during RV ejection, the required linear contraction of the PAM was determined to be 25%.[5,9,14] This contraction works against the elevated hemodynamic pressure in the RV and the afterload in the pulmonary artery. In contrast to previously suggested PAMs for cardiac support that are actuated at pressures close to atmospheric pressure in the chest cavity, the RVED operates inside the heart. During RHF blood pressure in the RV and pulmonary artery can reach 70 mmHg. This pressure would diminish the relative inflating pressure of the RVED internal bladder compromising PAM contractibility. Accordingly, the RVED was required to exert contraction forces higher than that required for external cardiac support devices (50 N).

The inner and outer bladder (0.3 and 0.25 mm thick TPU respectively) were fabricated as previously described.[21] To avoid air leaks the inner bladder was heat sealed to its airline (TPU, Eldon James Corporation) with a custom milled aluminum mold heated to 180 °C for 40 s. Injection molding techniques were used to fabricate the proximal and distal part of the RVED device. A two-step process was employed using 3-D printed molds (Vero material, Objet Connex 500) as shown in Figs. 2. Figures 2a and 2b show the injection mold process for the distal end (9.8 mm diameter, 4 mm length molded part). Figure 2c shows the injection molding process for the proximal end (9.8 mm diameter, 40 mm length molded part). To ensure homogenous polymer formation each injection mold had an overflow tract, and the resin was cured at each step under 400 kPa pressure for twelve hours. The final device is shown in Fig. 2d.

Septal and Free Wall Anchoring Systems—For the septal anchoring system, we defined the following requirements: linear deployment across the IVS without creating an interventricular shunt; ability to withstand the force generated by the linear actuator; ultrasound compatibility; ability to involve an adequate area of the septum in its approximation toward the RV free wall.

The anchor consists of collapsible wings that were radially bound on a stainless-steel base around a threaded core pin, such that the wings can only unfold up to 90° in order to avoid folding backwards during the device actuation (Figs. 3a and 3b) To provide enhanced ultrasound compatibility and withstand high dynamic forces, the wings were fabricated from a high modulus polymer (Polyether ether ketone—PEEK—7 mm × 1.5 mm × 2 mm). A superelastic nickel-titanium (Nitinol) wire ring was attached through the free ends of the wings to form a circular spring system and enable self-expanding deployment. A second retrievable Nitinol release wire was attached to the ring allowing controlled device repositioning (see Supplementary Video). Once the wings are deployed in the appropriate position and laid flat on the left side of the IVS, a T shaped cap is secured on the center pin of the anchor from the RV side. The IVS is then sandwiched between the open wings on the left side and the cap on the right side. Enclosing the IVS in this manner seals the access area in the IVS and prevents intraventricular shunting.

To secure the actuator to the RV free wall, and to prevent blood loss during device actuation, we used a tubular RV free wall anchor (Fig. 3b). The free wall was sandwiched between the inner lip of the anchor and the external purse string suture. Additionally, an O-ring positioned between the anchor shaft and the air supply lines sealed the device from inside preventing blood loss. A radially positioned stud screw fixed the RV free wall anchor to the air supply lines. The entire custom design of the anchor was 3D printed in Vero material (Objet Connex 500).

Actuation Controller—A custom software interface (Fig. 3c) was developed (LabVIEW, National Instruments) using an X-Series Data Acquisition Box (DAQ) (National Instruments). Pressurization of the internal bladder as well as the application of negative relative pressure to the outer bladder were independently programmable by setting desired pressure levels, actuation periods and frequencies. Utilizing two electro-pneumatic regulators (ITV series, SMC) coupled to separate solenoid valves (VQ series high-flow 3 way, SMC) the control system delivered compressed air and vacuum from standard wall sources to the actuator. Synchronization to the native cardiac cycle was established employing a pacemaker (5342, Medtronic Inc.) which simultaneously sent an electrical signal to the RV and to the controller.

Component Optimization and Force Characterization—A single filament braided PET mesh with maximal diameter of 26 mm (Flexo PTO 0.25, Techflex Inc.) and 40 mm in length was selected. Three mesh/bladder combinations were manufactured using the TPU inner bladders 20, 30 and 40 mm in length placed inside the mesh. The bladders were detached from the distal end of the mesh.

Three specimens of each combination were actuated dynamically for 250 ms contraction period at 1.25 Hz (simulating physiological ranges of 75 beats per minute) while input pressures were systematically increased from 20 to 240 kPa. Actuation was video recorded at 250fps. Single frames at maximal contraction and relaxation were extracted, and linear contraction was calculated using image-processing software (ImageJ, National Institutes of Health).

The highest performing mesh/bladder combination from this experiment was then tested (n = 3) to measure the force/contraction behavior with a mechanical tensile tester (Instron 5566, Instron, Norwood, USA). Specimens were secured in the fixation clamps of the tester and peak forces were recorded at contraction levels from 0 to 35% under similar dynamic actuation as in the contraction study at 1.25 Hz. The input pressure was systematically increased from 34 to 275 kPa.

To quantify extension forces of the external bladder, the final actuator design was tested in a tensile tester. After device fixation in the testing machine a vacuum pressure of 80 mmHg was dynamically applied to the outer bladder (Fig. 1e) and the resulting force was recorded.

Performance Characterization in Ventricular Simulator—To characterize device functionality under the envisaged hemodynamic conditions, we designed a ventricle simulator. The simulator consisted of two opposing silicone membranes supported by an acrylic frame (Fig. 4a). The membrane material (Ecoflex00-30, Smooth-on Inc.) was chosen to imitate the stiffness of heart tissue[23] and the wall thickness was matched to the respective thickness of the RV free wall (5 mm) and the IVS (15 mm) as determined from measurements in porcine hearts (n = 3). The total surface area of the silicone walls was designed to match the total surface area in a typical RV (130 cm^2) as calculated from CT scan data of a human heart and examinations of porcine hearts (n = 3). We used water in lieu of blood and measured the volumes ejected *via* a 10 mm wide calibrated outflow tube. Simulator chamber pressure was monitored in real-time (ArgoTrans model 2 Neonatal macro-drip transducer, Argon medical; Surgivet, Smith Medical). Afterloads were varied from 10 to 70 mmHg by changing the height of the water column in the outflow tube. Since there was no valve between the outflow tube and the chamber, afterload pressure was equal to chamber pressure prior to actuation. The device was actuated at 1.25 Hz (simulating physiological frequencies of 75 beats per minute) and input pressures were systematically increased from 20 to 275 kPa. Pressurization periods ranged from 100 to 300 ms to assess the effect of actuation period on ejected volumes. The experiment was video recorded, and single frames were extracted for analysis. Ejection volume and chamber pressure were measured directly. Linear contraction of the actuator was calculated (ImageJ software) employing a laser engraved millimeter scale in the acrylic frame for calibration (Fig. 4b).

Prior to *in vivo* device testing we conducted a durability study of the RVED in the ventricular simulator for 6 h (n = 5). A duration of 6 h was chosen to assure that the device would be suitable for safe use in an intracardiac position during the *in vivo* evaluation. The simulator was filled with 0.9% saline solution (temp = 36.5 °C), and the device was actuated for 250 ms periods at 1.25 Hz and maximal pressures of 275 kPa. Visual inspection every 30 min was conducted to detect bubble formation in the water bath or any water in the airlines. At the end of each experiment, the actuators were disassembled and inspected for wear.

In Vivo Evaluation

To assess device placement and anchoring under echocardiography guidance we used female Yorkshire pigs (n = 4). We then evaluated feasibility of device performance in a porcine RHF model (n = 1). The animals received humane care in accordance with the 1996 Guide

for the Care and Use of Laboratory Animals recommended by the US National Institute of Health. The experimental protocol was approved by the Boston Children's Hospital Institutional Animal Care and Use Committee.

The procedures were performed under general anesthesia, as previously described.[25] The heart was approached *via* midline sternotomy and flow probes were placed around the main pulmonary artery (PA) and the ascending aorta (Transonic PS series). RV, PA and systemic pressures were measured directly in real-time (Argo Trans probes).

Echocardiography Guided Implantation into Beating Heart—The feasibility of RVED implantation under 2D and 3D echocardiography guidance on the beating heart was evaluated in four pigs. The target area for the RVED placement was identified using echocardiography guidance. For the septal anchor placement, we chose the mid-muscular ventricular septum. By positioning the device directly inferior to the septal papillary muscle, the chance of affecting the atrioventricular nodal branches of the right coronary artery or the first septal perforator branches of the left anterior descending coronary artery is minimized.[13] Additionally, device placement in this area avoids the conduction system, the branches of the bundle of His,[3] thus minimizing the risks associated with this placement. For the RV free wall anchor, the area just anterior to the mid portion of the anterior papillary muscle was selected.

After heparin administration (300 U/kg IV, activated clotted time above 250 s), a purse-string suture was placed on the RV free wall, and a marked needle was introduced into the RV and then advanced into the LV through the IVS. A guide wire was introduced into the LV through the needle and the needle was then removed. The access area in the free wall and septum was enlarged by a series of dilators over the wire. The LV part of the septal anchor in the folded configuration, attached to a stainless-steel pusher rod (Fig. 3a), was delivered *via* a valved 20Fr introducer sheath (Cook medical) and opened (Fig. 3b) on the LV side of the IVS such that the opened wings lay flat against the septum. Echocardiography guidance was used to avoid damaging mitral valve chordae apparatus during anchor placement, and retractable control of wing folding and unfolding facilitated precise positioning. Next, a custom made 12 mm introducer sheath with the RV part of the septal anchor was delivered into the RV *via* the same access over the pusher, and the RV part of the septal anchor was screwed onto the threading of the LV part, which completed the septal anchor placement. Then, the pusher was replaced with the actuator (Fig. 3b), the sheath was withdrawn, and the RV free wall anchor was placed into the position and secured within the purse string suture. The device was then connected to the air and vacuum source and operated using the controller.

Functional Evaluation in the Model of End-Stage RHF Resulted from Volume Overload—In order to determine performance of the RVED in conditions of end-stage RHF resulting from volume overload, *in vivo* evaluation under cardiopulmonary bypass (CPB) was performed in one animal. Use of CPB was necessary to safely simulate a status of RV volume overload while leaving the systemic circulation intact. General anesthesia was established as described above. A midline sternotomy was performed, and CPB was established such that venous return was collected from the superior vena cava and the

inferior vena cava, and arterial inflow was returned to the right femoral artery. During CPB fentanyl (50–200 m/kg) and midazolam (0.2 mg/kg) were administered for anesthesia. The animals were cooled to 32 °C, at which point the ascending aorta was cross-clamped and the heart was arrested by anterograde delivery of cold cardioplegia solution (del Nido solution). The right atrial appendage was opened and the RVED was implanted under direct vision after which the right atriotomy was closed, the heart was de-aired, the animal was rewarmed and the aortic cross-clamp was removed to restart heart contraction. The animal was maintained on 80% CPB flow. By controlling the amount of the venous return into the right side of the heart (CVP up to 16 mmHg), we could generate RV volume overload in controllable fashion causing RHF. The hemodynamic effect of the RVED actuation was assessed by measuring PA and aortic flow, PA, RV and systemic pressures. The device was actuated in synchrony with heart contractions that were triggered by epicardial pacing; the same pacing signal was sent to the heart and to the controller for triggering the device. During the device actuation, the data was recorded for 10 min. Data were averaged over 10 cardiac cycles for analysis.

RESULTS

Actuator Shortening and Contraction Forces

Contraction behaviors at varying inner bladder to mesh lengths are summarized in Fig. 5a Reducing bladder to mesh length ratio led to improved linear contraction at lower actuation pressures. PAM with a bladder length of 50% compared to total mesh length reached 25% contraction at 60 kPa, and the maximal contraction was 31% at 240 kPa. Actuators with 75% bladder length to mesh length ratio reached 25% contraction at 120 kPa, 28% contraction at 140 kPa and improved their maximal linear contraction to 31% at 241 kPa. Specimens with equal bladder and mesh length reached lower contractions at all actuation pressures with the maximal contraction of 27% at 276 kPa (Fig. 5a). We observed material failure of specimens with 50% length ratio at input pressures of 276 kPa but not with 75% or 100% ratios. For the final design we thus chose a bladder to mesh ratio of 75%.

Generated force to contraction behavior is summarized in Fig. 5b. A peak contraction force of 140 N was generated by the device at 276 kPa. At 25% contraction, at least 10 N of force could be generated by any input pressure above 69 kPa. Diastolic extension of the actuator resulted in 6 N extension force.

Device Performance in Ventricular Simulator

Device performance for various input parameters are summarized in Fig. 6. The device was capable of ejecting 21 mL of volume at 10 mmHg afterload which dropped 61% to 8 mL at 70 mmHg afterload (Fig. 6a). Device actuation was able to generate pressure in the simulator chamber of 20–28 mmHg (Fig. 6b). Maximal device shortening decreased from 30% contraction at an afterload of 10 mmHg to 26% at an afterload of 70 mmHg (213.5%) (Fig. 6c). Increasing the input pressure above 180 kPa lead to minor improvements in ejection volume and generated pressure. At 1.25 Hz increasing the contraction period from 100 to 250 ms augmented ejected volume by 30% while additional increase to 300 ms did not result in higher ejected volume. This implied an optimal actuation period of 250 ms. All

components of the device (balloon, mesh, airline and bonding materials) were found to be intact upon examination after completion of the durability studies.

Echocardiography Guided Implantation into the Beating Heart

Echocardiography provided clear visualization of the anatomic structures and the septal anchor during device placement (Fig. 7a). The device was successfully implanted across the RV in all four animals (Figs. 7b and 7c). The deployment was typically completed in 20 min. No damage to the intracardiac structures and no major blood losses were observed. The linear actuator was securely connected to the septal and the RV anchoring systems in all animals. There was no blood loss at the RV access throughout the device operation. One animal had an episode of heart block after device placement, which required therapeutic use of a pacemaker. Postmortem evaluation of the hearts demonstrated successful sandwiching of the septum by the septal anchor in all cases (Fig. 7d) without gross damage to the heart.

In all deployment experiments, normal hemodynamics were preserved. There was no improvement in mean PA flow (1.6 l/min/SD 0.79 vs. 1.6 l/min/SD0.93 respectively), mean RV pressure (9.8 mmHg/SD4.9 vs. 10.1 mmHg/SD0.4), and mean PA pressure (17.9 mmHg/SD3.1 vs. 18.1 mmHg/SD2.8 respectively), over native RV function upon device actuation in these hearts with normal size and function.

Functional Evaluation in the Model of End-Stage RHF Resulted from Volume Overload

The device successfully augmented RV ejection (Fig. 8). Systolic RV pressure decreased from 21 mmHg baseline to 3.5 mmHg (17%) during RHF and was recovered to 29 mmHg (138%) during RVED assistance (Figs. 8a and 8b). Diastolic RV pressure increased during RHF from 10 mmHg baseline to 24 mmHg and was increased to 28 mmHg during the device actuation (Fig. 8b). Systolic PA pressure decreased from 10 mmHg baseline to 1.6 mmHg (17%) during RHF and was recovered to 8.8 mmHg (89%) by the RVED (Figs. 8c and 8d). Right ventricular output (PA flow) dropped during the RHF from 2.4 L/min at healthy baseline to non-pulsatile 0 L/min during CPB (not registered by the flow probe). RVED actuation clearly increased the PA flow to 0.2 L/min (8% of healthy baseline) (Figs. 8e and 8f).

DISCUSSION

We demonstrate an alternative approach of assisting the failing ventricle using a device that is designed to augment native ventricular blood ejection. Augmentation is achieved by approximating the ventricular free wall and the IVS in synchrony with the cardiac cycle. This strategy is especially relevant to RHF patients with IVS flattening or right-to-left septal shift.[6,27] Currently there are no small RVAD that can be rapidly deployed that also provide pulsatile flow augmentation to the native RV contraction. The advantages of pulsatile flow have been greatly studied for LVADs. Pulsatile VADs have been more or less disfavored because of their large size and propensity for thrombi formation, especially at the one-way flow valves. The proposed RVED is low profile and easily deployed on the beating heart using echocardiography guidance, the device achieves pulsatile flow augmentation while

minimizing surface area of artificial material in contact with blood. The maximal surface area of the device at the fully actuated state that in the blood flow path is 2500 mm.[2]

The concept of using soft robotic actuators mimicking contractile function of ventricular walls has been previously described by our group.[19,22,23] The PAM actuators are lightweight, have fast response times, and are tunable to match physiologic requirements of the heart.[19,21] In contrast to previous designs that provide biventricular support using an enclosing sleeve,[22,23] the RVED is specifically conceived to address the structural changes that are seen in advanced right heart failure.[6,10,20,27] In this study, by employing a combination of soft robotics and precision engineering we developed a device that is small enough to be safely deployed inside the beating heart.

We have demonstrated that use of TPU internal bladders detached from the distal point of the mesh and reduction of the bladder to mesh/ratio can lead to improved actuator shortening but there is a threshold below which actuator weakness is encountered. We have also demonstrated that the proposed design, at dynamic actuation of 1.25 Hz and input pressures of above 69 kPa, produced forces adequate to overcome the expected physiologic hemodynamic resistance. McKibben PAMs intrinsically have self-limiting force–length curves similar to human muscle.[7,8,16] This makes them one of the safest actuators to use for this purpose, because the linear force applied decreases with contraction such that the maximal force applied to the tissue will be as required to initiate contraction and not the total maximum force measured using a tensile tester.

Using a ventricular simulator, we demonstrated that it was feasible to obtain up to 21 mL of ejection volume from the device while causing a linear approximation of at least 26%. The device was operated at 275 kPa for up to 6 h under physiological loads without undue fatigue further showing suitability to intracardiac use.

We have demonstrated the feasibility of device implantation into the beating heart under echocardiography guidance. In a model of end-stage RHF resulting in no ejection from the ventricle, the RVED restored ventricular pressures to baseline healthy values and resulted in 8% augmentation of RV ejection, which may make a clinically significant difference in patients with RHF. Van de Veerdonk *et al.* demonstrated that in patients with PA hypertension responding to therapy with an improvement in pulmonary ventricular resistance, improvement in RV ejection of 10% over the follow up period was significantly associated with survival.[26] Contraindication to use of this device would be biventricular failure, since the device augments only the RV contraction. Patients with ventricular septal defects that would preclude safe implantation of the anchoring system would not be candidates for this device. Lastly, patients with severe tricuspid or pulmonary valve regurgitation may not benefit from use of this device.

The main challenges in using soft robotic intracardiac implants include the risk of air embolism in the case of a leak from the pneumatic circuit, and requirement of perfect synchronization of the device actuation with native heartbeat. Clinical experience with intra-aortic balloon pumps, that are placed inside the aorta and actuated with inert gas, suggests that the risk of air leak can be significantly mitigated with engineering design.[24] In our

current prototype, we have addressed the issue by customizing the PAM incorporating a second external protective bladder that is not pressurized during the device actuation. In addition, vacuum is applied to the external bladder during diastole, which may capture escaped air bubbles from the inner bladder serving as an additional protective feature. An additional sensor system that detects pressure changes in the bladders in real time is necessary. In this feasibility study, we synchronized the device actuation with the cardiac cycle by simultaneously pacing both the RV and the device. Further optimization of a synchronization closed loop algorithm using triggering off an EKG signal, RV pressure curve and flow curve will improve synchronization.

While we describe the device design and demonstrate functional feasibility in one animal, further animal studies are required to fully elucidate the physiological impact of this approach. The RVED is fixed at distinct points on the RV free wall and at the septum, and therefore the device contributes solely to RV free wall ventricular septum approximation. In normal or thin walled RV, ballooning of the free wall areas not involved by the device hypothetically limits the effectiveness of the approach. Conversely, implantation of the device into a hypertrophied RV would improve augmentation in comparison with the results we have observed in the normal ventricle. Another strategy to improve ejection augmentation would be the placement of additional actuator(s) to affect RV longitudinal shortening. While no macroscopically detected damage was noted on the RV free wall and the ventricular septum as a result of the device actuation (Fig. 7d), histological examination following longer periods of actuation will be required. The impact of the device placement and actuation on the left ventricular function will also need to be systematically studied. Furthermore, material design optimization for blood compatibility would be required prior to clinical use. All these considered, the proposed device was successfully designed for echocardiography guided implantation and tested *in vitro* and *in vivo*. It represents a promising approach for the support of the failing RV. It may be especially well situated for the rapid establishment of short-term pulsatile RV ejection augmentation.

Supplementary Material

Refer to Web version on PubMed Central for supplementary material.

Acknowledgments

This work was supported in part by the NIH/NHLBI NCAI Boston Biomedical Innovation Center Pilot Grant (NVV), the DoD CDMRP Discovery Award W81XWH-15-1-0248 (NVV), the Wyss Institute for Biologically Inspired Engineering and the Harvard Paulson School of Engineering and Applied Sciences.

References

1. Anderson MB, Goldstein J, Milano C, Morris LD, Kormos RL, Bhama J, Kapur NK, Bansal A, Garcia J, Baker JN, Silvestry S, Holman WL, Douglas PS, O'Neill W. Benefits of a novel percutaneous ventricular assist device for right heart failure: the prospective RECOVER RIGHT study of the Impella RP device. J. Heart Lung Transplant. 2015; 34:1549–1560. [PubMed: 26681124]
2. Anderson MB, O'Brien M. Use of the impella 2.5 microaxial pump for right ventricular support after insertion of heartmate II left ventricular assist device. Ann. Thorac. Surg. 2013; 95:e109–e110. [PubMed: 23608288]

3. Anderson RH, Yanni J, Boyett MR, Chandler NJ, Dobrzynski H. The anatomy of the cardiac conduction system. Clin. Anat. 2009; 22:99–113. [PubMed: 18773472]
4. Auger DA, Zhong X, Epstein FH. Mapping right ventricular myocardial mechanics using 3D cine DENSE cardiovascular magnetic resonance. J. Cardiovasc. Magn. Reson. 2012; 14:1. [PubMed: 22226320]
5. Bramos D, Tsirikos N, Kottis G, Pamboucas C, Kostopoulou V, Trika C, Ikonomidis I, Toumanidis S. The acute effect of an echo-contrast agent on right ventricular dimensions and contractility in pigs. J. Cardiovasc. Pharmacol. 2008; 51:86–91. [PubMed: 18209573]
6. Buckberg GD. Restore Group. The ventricular septum: the lion of right ventricular function, and its impact on right ventricular restoration. Eur. J. Cardio-Thorac. Surg. 2006; 29:S272–S278.
7. Chou CP, Hannaford B. Static and dynamic characteristics of McKibben pneumatic artificial muscles. IEEE. Int. Conf. Robot. Autom. 1994; 1:281–286.
8. Chou CP, Hannaford B. Measurement and modeling of McKibben pneumatic artificial muscles. IEEE Trans. Robot. Autom. 1996; 12:90–102.
9. Geva T, Powell AJ, Crawford EC, Chung T, Colan SD. Evaluation of regional differences in right ventricular systolic function by acoustic quantification echocardiography and cine magnetic resonance imaging. Circulation. 1998; 98:339–345. [PubMed: 9711939]
10. Haddad F, Doyle R, Murphy DJ, Hunt SA. Right ventricular function in cardiovascular disease, part II: pathophysiology, clinical importance, and management of right ventricular failure. Circulation. 2008; 117:1717–1731. [PubMed: 18378625]
11. Hsu DT, Pearson GD. Heart failure in children part I: history, etiology, and pathophysiology. Circ Heart Fail. 2009; 2:63–70. [PubMed: 19808316]
12. Hsu P, Parker J, Egger C, Autschbach R, Schmitz-Rode T, Steinseifer U. Mechanical circulatory support for right heart failure: current technology and future outlook. Artif. Organs. 2012; 36:332–347. [PubMed: 22150419]
13. James TN, Burch GE. Blood supply of the human interventricular septum. Circulation. 1958; 17:391–396. [PubMed: 13511658]
14. Lai WW, Gauvreau K, Rivera ES, Saleeb S. Accuracy of guideline recommendations for two-dimensional quantification of the right ventricle by echocardiography. Int. J. Cardiovasc. Imaging. 2008; 24:691–698. [PubMed: 18438737]
15. Larose E, Ganz P, Reynolds HG, Dorbala S, Di Carli MF, Brown KA, Kwong RY. Right ventricular dysfunction assessed by cardiovascular magnetic resonance imaging predicts poor prognosis late after myocardial infarction. J. Am. Coll. Cardiol. 2007; 49:855–862. [PubMed: 17320743]
16. Leclair J, Doumit M, McAllister G. Analytical stiffness modeling and experimental validation for a pneumatic artificial muscle. ASME. 2014
17. Markel TA, Wairiuko GM, Lahm T, Crisostomo PR, Wang M, Herring CM, Meldrum DR. The right heart and its distinct mechanisms of development, function, and failure. J. Surg. Res. 2008; 146:304–313. [PubMed: 18036544]
18. Meyer P, Filippatos GS, Ahmed MI, Iskandrian AE, Bittner V, Perry GJ, White M, Aban IB, Mujib M, Dell'Italia LJ, Ahmed A. Effects of right ventricular ejection fraction on outcomes in chronic systolic heart failure. Circulation. 2010; 121:252–258. [PubMed: 20048206]
19. Obiajulu SC, Roche ET. Soft pneumatic artificial muscles with low threshold pressures for a cardiac compression device. ASME. 2013
20. Park E, Mehandru N, Beltran TL. An intraventricular soft robotic pulsatile assist device for right ventricular heart failure. J. Med. Dev. 2014; 8:020908.
21. Roche ET, Horvath MA. Design and fabrication of a soft robotic direct cardiac compression device. ASME. 2015
22. Roche ET, Horvath MA, Wamala I, Alazmani A, Song S-E, Whyte W, Machaidze Z, Payne CJ, Weaver JC, Fishbein G, Kuebler J, Vasilyev NV, Mooney DJ, Pigula FA, Walsh CJ. Soft robotic sleeve supports heart function. Sci. Transl. Med. 2017; 9:3925.
23. Roche ET, Wohlfarth R, Overvelde JTB, Vasilyev NV, Pigula FA, Mooney DJ, Bertoldi K, Walsh CJ. A bioinspired soft actuated material. Adv. Mater. 2014; 26:1200–1206. [PubMed: 24227698]

24. Stone GW, Ohman EM, Miller MF. Contemporary utilization and outcomes of intra-aortic balloon counterpulsation in acute myocardial infarction: the benchmark registry. J. Am. Coll. Cardiol. 2003; 41:1940–1945. [PubMed: 12798561]

25. Vasilyev NV, Martinez JF, Freudenthal FP. Three-dimensional echo and videocardioscopy-guided atrial septal defect closure. Ann. Thorac. Surg. 2006; 82:1322–1326. [PubMed: 16996927]

26. van de Veerdonk MC, Kind T, Marcus JT, Mauritz G-J, Heymans MW, Bogaard H-J, Boonstra A, Marques KMJ, Westerhof N, Vonk-Noordegraaf A. Progressive right ventricular dysfunction in patients with pulmonary arterial hypertension responding to therapy. J. Am. Coll. Cardiol. 2011; 58:2511–2519. [PubMed: 22133851]

27. Voelkel NF, Quaife RA, Leinwand LA, Barst RJ, McGoon MD, Meldrum DR, Dupuis J, Long CS, Rubin LJ, Smart FW, Suzuki YJ, Gladwin M, Denholm EM, Gail DB. L. National heart and blood institute working group on cellular and molecular mechanisms of right heart failure. Right ventricular function and failure: report of a National Heart, Lung, and Blood Institute working group on cellular and molecular mechanisms of right heart failure. 2006

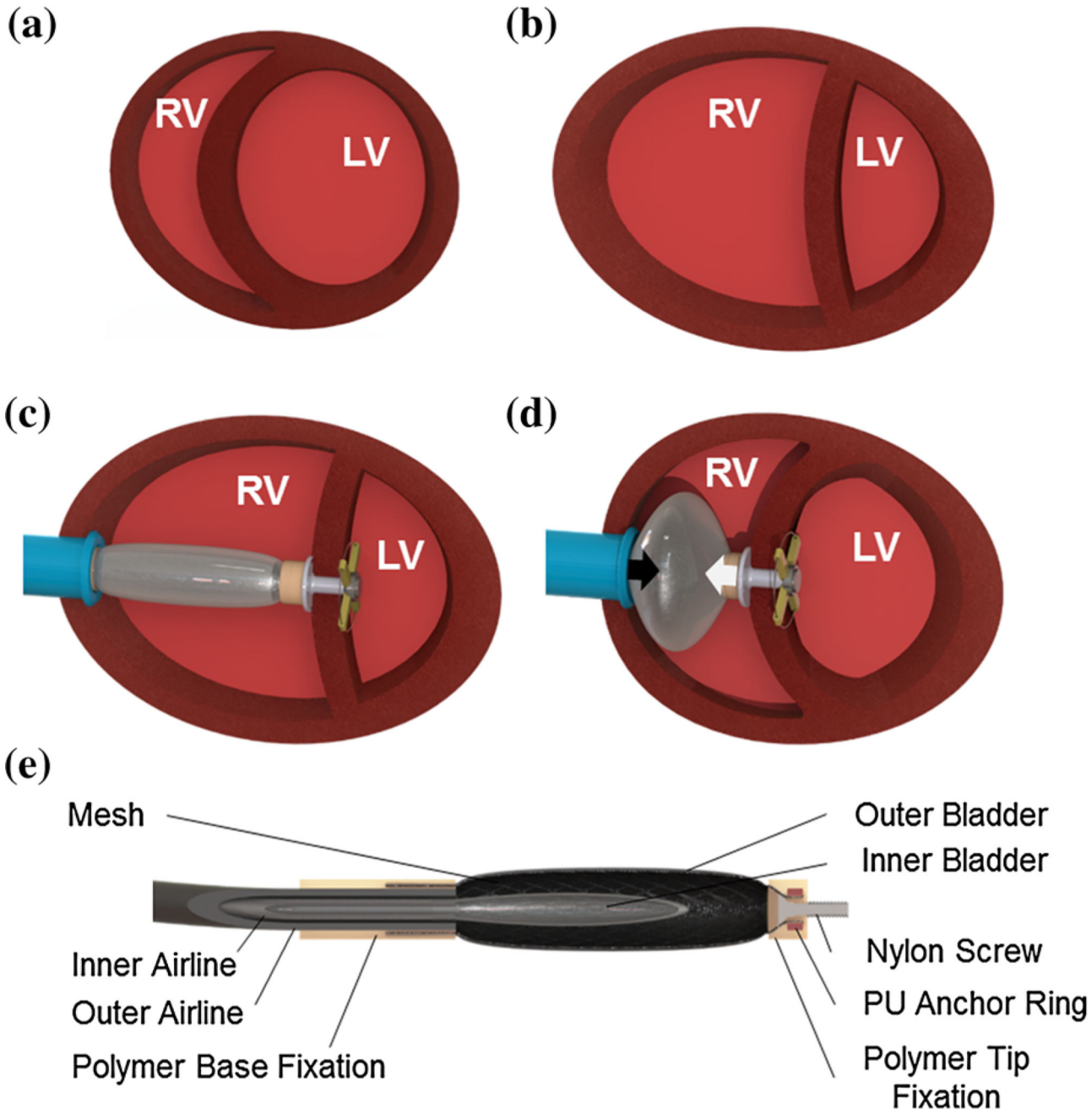

FIGURE 1.

(a) Illustration of the cross section of a healthy heart, in comparison with (b) a heart with right heart failure characterized by a dilated RV, deformed LV and ventricular septal right-to-left shift. (c) Schematic illustration of the right ventricular ejection device implanted in a heart with right heart failure. (d) The actuation of the pneumatic artificial muscle results in linear approximation (black arrows) of the ventricular septum and the RV free wall. (e) Schematic illustration of the linear actuator cross section depicting the components.

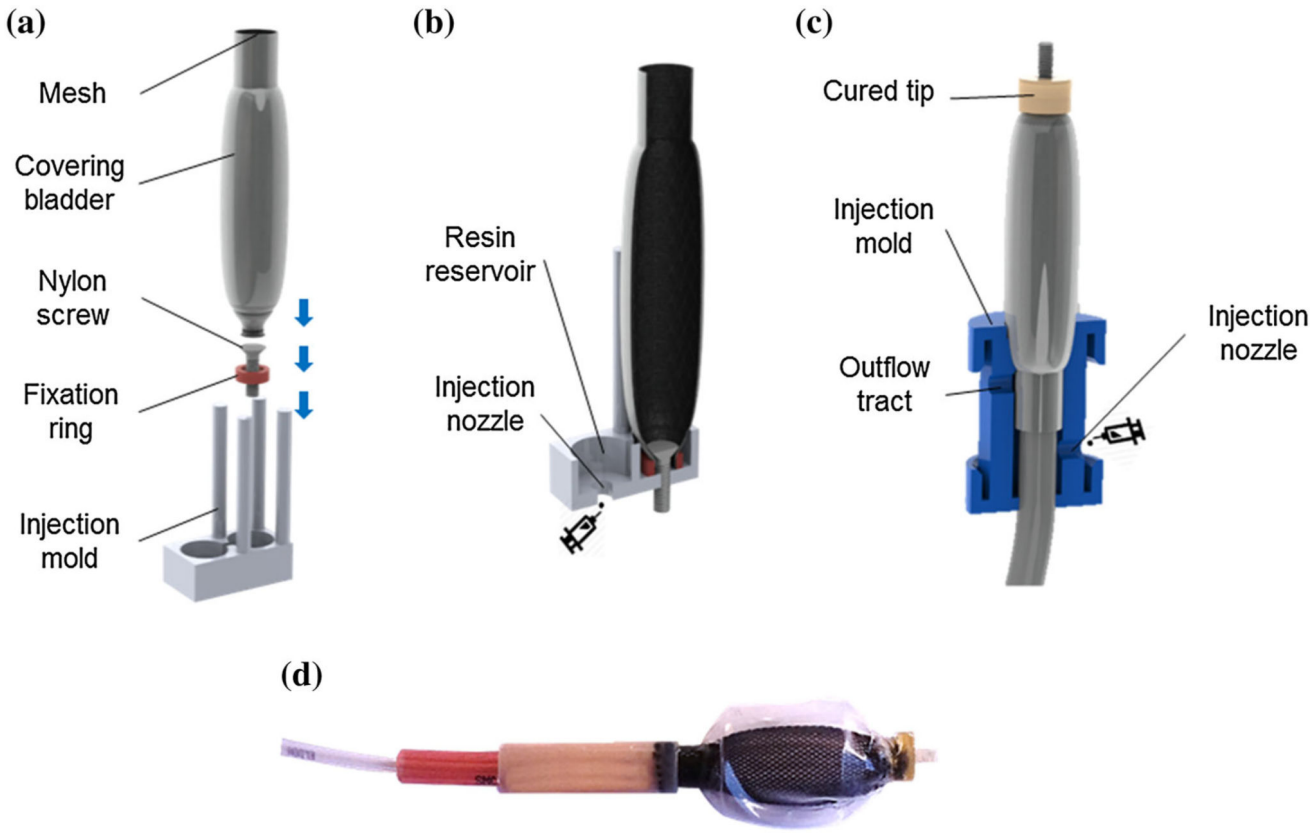

FIGURE 2.

Schematic of the device fabrication process: (a) device tip: outer bladder and mesh are collapsed over a nylon screw and fixed by a TPU locking ring before positioning in the injection mold; (b) cross section during injection molding; (c) device base: insertion of inner bladder together with supply tubes and polymer casting; (d) photo of finalized contraction device.

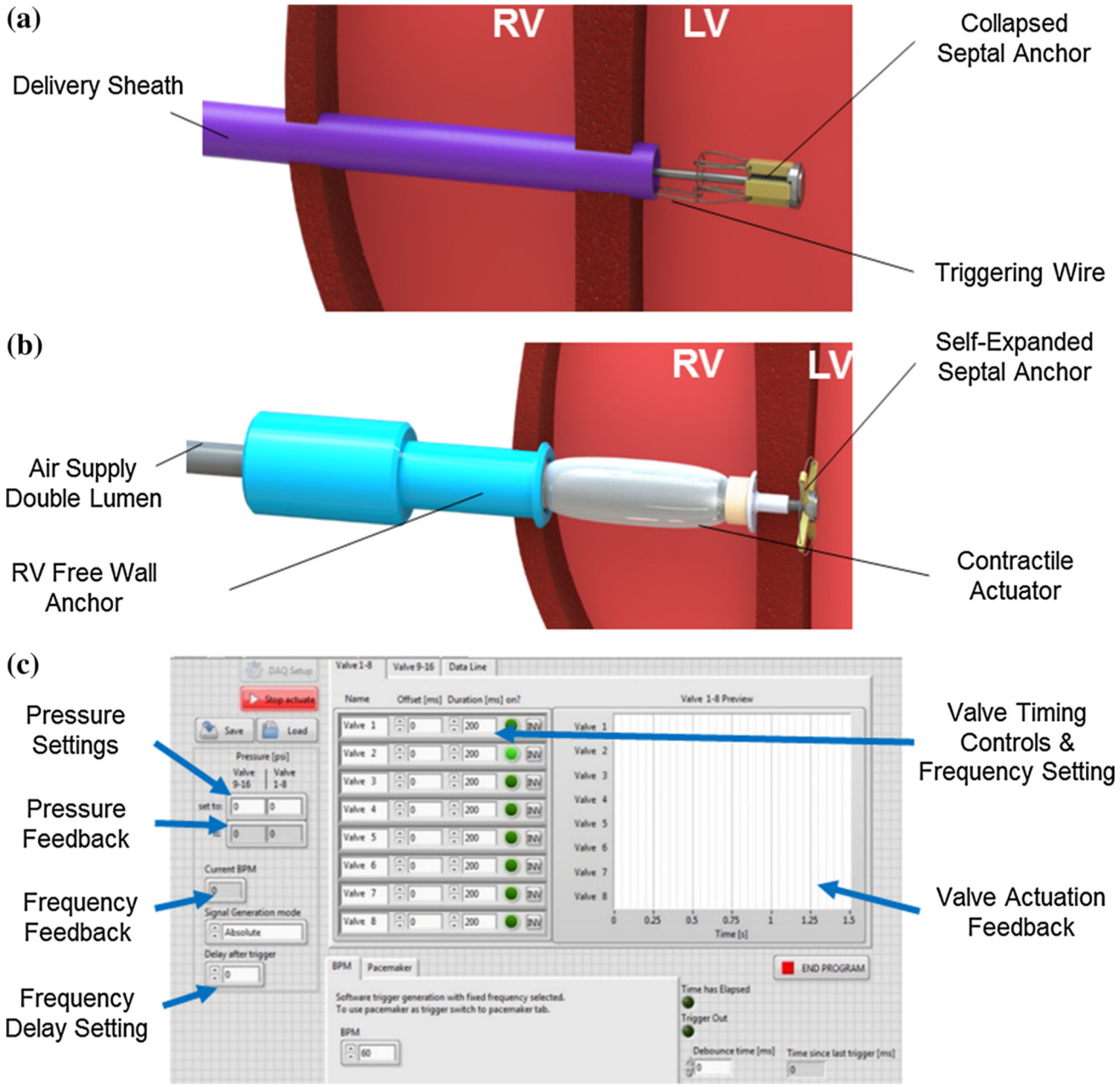

FIGURE 3.

(a) Illustration of the delivery of the collapsed septal anchor into the LV in the beating heart and (b) of complete ejection device positioned in the RV. (c) Custom software interface to control device actuation.

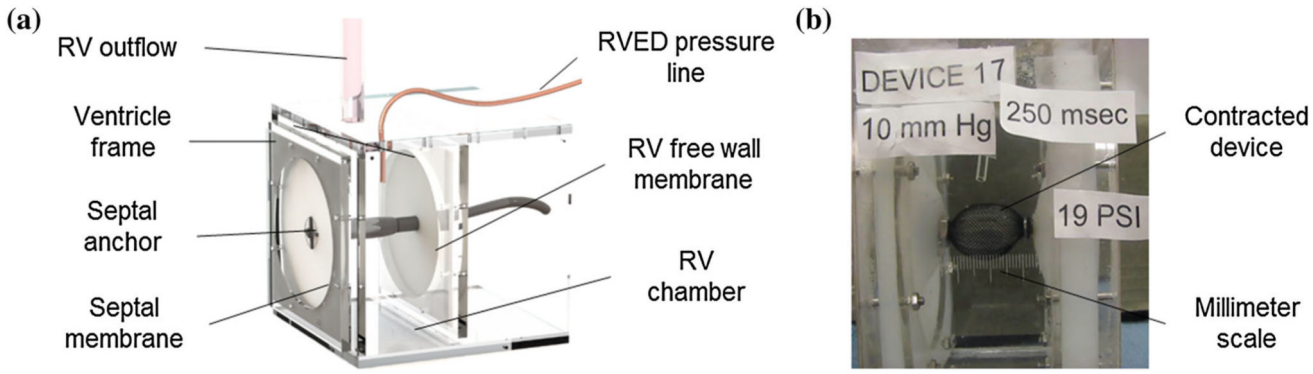

FIGURE 4.

(a) *In vitro* testing of the RVED in a simplified RV simulator; (b) contracted device is approximating the simulated septum and free wall.

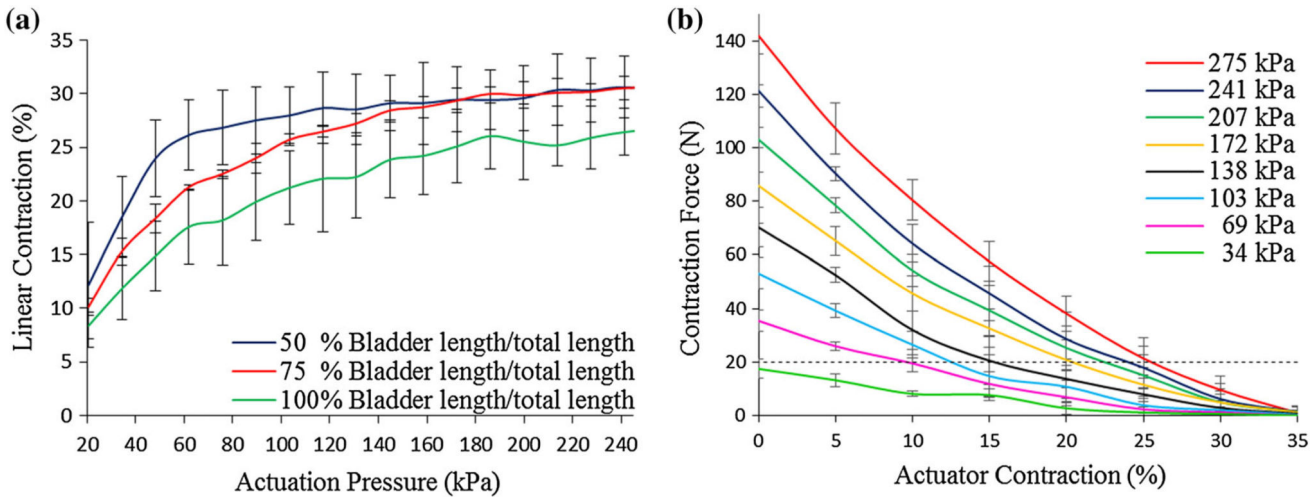

FIGURE 5.

(a) Contraction characterization at varying actuation pressure of PAM with varying inner bladder length at constant mesh length (40 mm). (b) Contraction vs. Force curve for final RVED (40 mm) at increasing actuation pressures. The targeted 20 N threshold line is indicated (black dotted line).

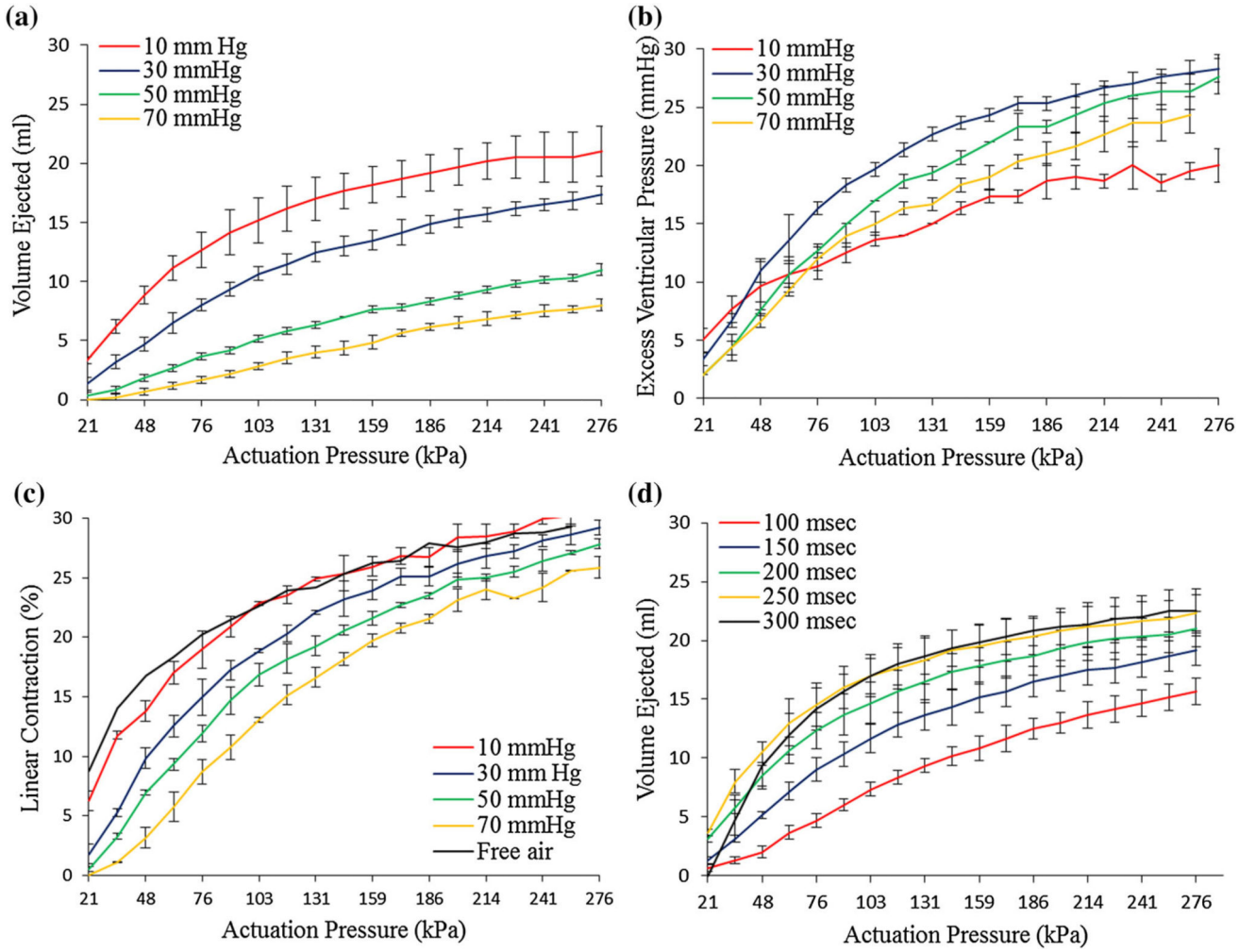

FIGURE 6.

(a) Ejected volume by device in ventricular simulator at increasing afterloads and actuation pressure. (b) Characterization of generated pressure in the ventricular simulator upon device actuation under varying afterloads and increasing actuation pressure. (c) Linear contraction of device under varying afterloads and increasing actuation pressure. (d) Ejected volume at varying actuation periods and increasing actuation pressure.

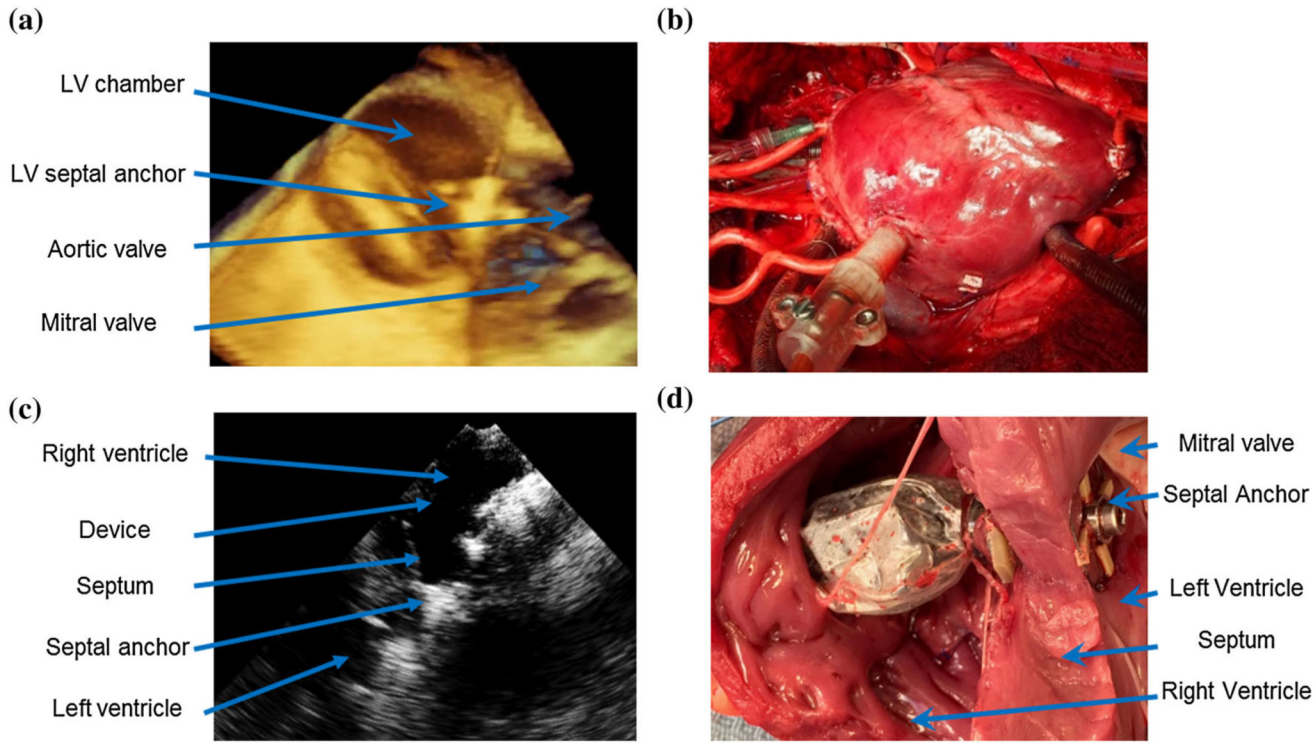

FIGURE 7.

(a) 3D echocardiography image showing the septal anchor during *in vivo* delivery in the beating heart after the controlled opening of the anchor wings inside the LV. (b) Photo of the successfully deployed device into a beating heart. (c) 2D echocardiography image showing implanted device inside RV and relation to the IVS. (d) Post mortem photo of the device successfully deployed into the beating heart displaying no visible damage to the septum.

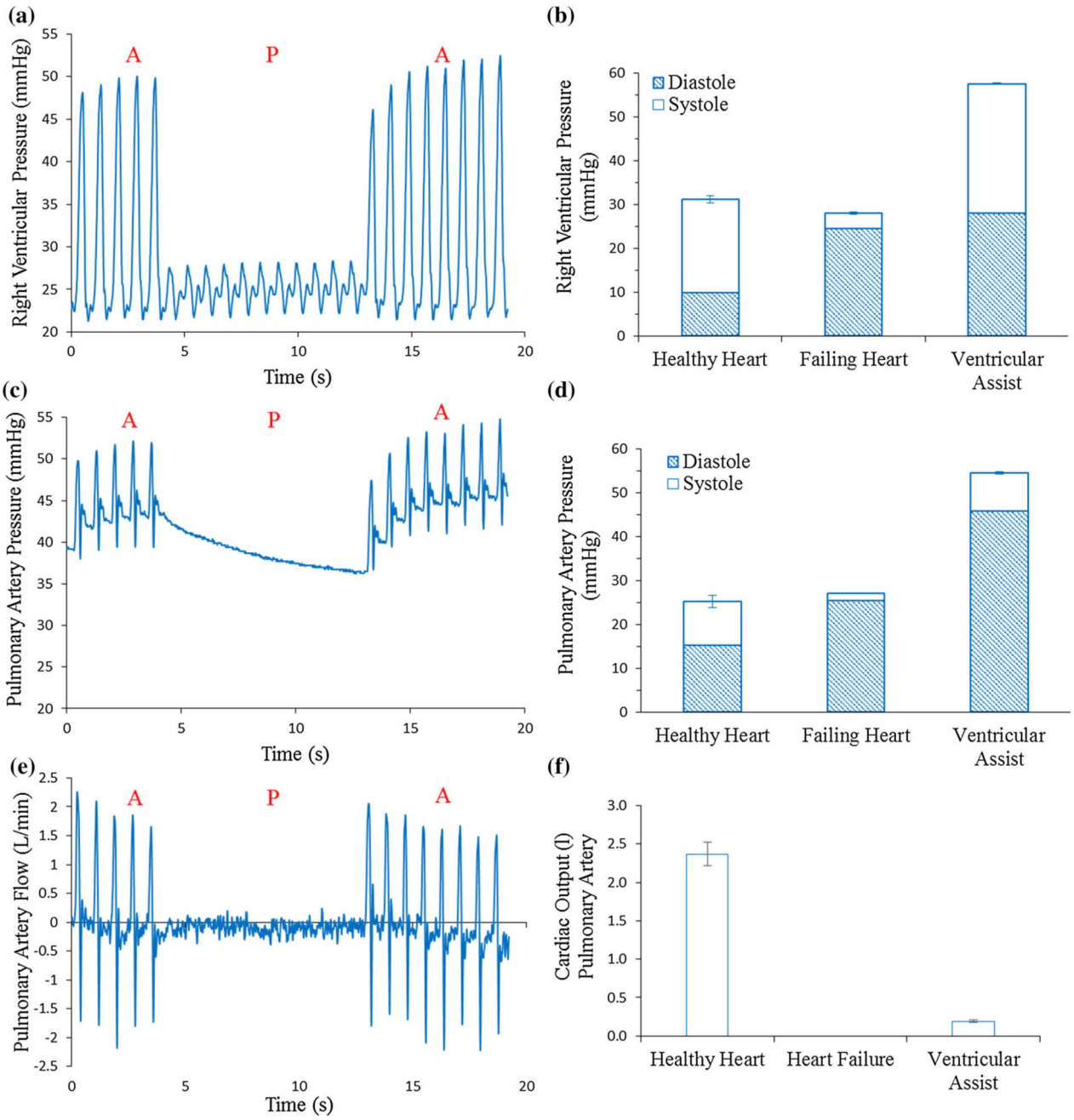

FIGURE 8.

RVED testing in RHF model resulting from volume overload. (a) Example of RV pressure showing periods of device actuation (A) and pause (P). (b) RV pressure in the healthy heart, the failing heart and the failing heart during device actuation conditions. (c) Example of PA pressure during heart failure showing periods of device actuation (A) and pause (P). (d) PA pressure comparing the healthy heart, the failing heart and the failing heart during device actuation conditions. (e) Example of PA flow during heart failure showing periods of device

actuation (A) and pause (P). (f) PA flow comparing the healthy heart, the failing heart and the failing heart during device actuation conditions.